

Fan Noise Prediction with Applications to Aircraft System Noise Assessment

Douglas M. Nark*

NASA Langley Research Center, Hampton, VA 23681-2199, U.S.A

Edmane Envia[†]

NASA Glenn Research Center, Cleveland, OH 44135, U.S.A

and Casey L. Burley[‡]

NASA Langley Research Center, Hampton, VA 23681-2199, U.S.A

This paper describes an assessment of current fan noise prediction tools by comparing measured and predicted sideline acoustic levels from a benchmark fan noise wind tunnel test. Specifically, an empirical method and newly developed coupled computational approach are utilized to predict aft fan noise for a benchmark test configuration. Comparisons with sideline noise measurements are performed to assess the relative merits of the two approaches. The study identifies issues entailed in coupling the source and propagation codes, as well as provides insight into the capabilities of the tools in predicting the fan noise source and subsequent propagation and radiation. In contrast to the empirical method, the new coupled computational approach provides the ability to investigate acoustic near-field effects. The potential benefits/costs of these new methods are also compared with the existing capabilities in a current aircraft noise system prediction tool. The knowledge gained in this work provides a basis for improved fan source specification in overall aircraft system noise studies.

I. Introduction

The prediction of aircraft engine noise, a primary source of sound from aircraft, is important for addressing the issues of community and cabin noise. Accurate fan source modeling was an issue identified in a previous study¹ aimed at coupling high fidelity codes to investigate the acoustic shielding benefits of a Hybrid Wing Body (HWB) configuration. Fan noise prediction methods vary from empirical to fully computational, with Computational Aeroacoustics (CAA) methods at the far end of the computational spectrum. Empirical methods are attractive since they tend to require minimal computer resources and run times. However empirical methods are limited in application in that they can not be confidently used for fan designs that deviate significantly from those upon which the empirical method is based.

In contrast, computational methods rely on first principles, and in some instances, phenomenological considerations of the noise generation and propagation processes. Such methods have been developed for a number of fan noise sources and specific configurations.²⁻⁵ The use of these methods requires more expertise than the empirical models and often require access to fairly detailed aerodynamic and geometric input parameters from independent measurements and computations. As such, these methods can require significantly more computer resources and run times compared to the empirical methods, but potentially offer a level of fidelity that allows more accurate assessment of current designs and development of noise reduction strategies.

This paper describes a further assessment^{5,6} of current fan noise prediction tools via comparison with measured sideline acoustic levels from a benchmark fan noise test. Specifically, an empirical method and a new coupled computational approach are used to predict rotor-stator interaction noise from a benchmark configuration. Rotor-stator interaction noise, which is the tone or broadband noise produced as a result of the interaction between the fan wakes and fan exit guide vanes, continues to be of interest since it can be a dominant engine noise source. In the sections to follow, the chosen empirical method, the Aircraft NOise Prediction Program (ANOPP),⁷ is described. The individual

*Research Scientist, Structural Acoustics Branch, Research & Technology Directorate, Member AIAA

[†]Research Aerospace Engineer, M.S. 54-3, 21000 Brookpark Road, Cleveland, OH 44135, AIAA Associate Fellow.

[‡]Senior Research Scientist, Aeroacoustics Branch, Research & Technology Directorate, Member AIAA

components of the computational approach, which are coupled here for the first time, are then discussed and the coupling process summarized. Comparisons of predictions in the far-field, as well as with sideline noise measurements, are performed to assess the relative merits of the two approaches. In particular, the potential benefits/costs of the new coupled computational approach are also compared with those of the existing empirical aircraft noise system prediction tool. The study is intended to give a view of the issues entailed in coupling the source and propagation codes, as well as provide insight into the capabilities of the tools in predicting the fan noise source and subsequent propagation and radiation. The knowledge gained in this work provides a basis for improved fan source specification in overall aircraft system noise studies.

II. Experimental Test Cases

The selected fan noise test cases for this study are taken from a previous assessment of fan noise prediction capabilities⁶ involving an ultra-high-bypass ratio fan stage called the NASA/PW Advanced Ducted Propulsor (ADP) Fan 1. The 22-inch diameter rotor was tested in the NASA Glenn 9-Foot by 15-Foot (9'x15') acoustic wind tunnel (see Figure 1) in which sideline, as well as in-duct, acoustic measurements were acquired. The ADP fan,^{8,9} the cross-section of which is shown in Figure 2, has a relatively low stage pressure ratio of 1.29 and a subsonic design corrected tip speed of 840 ft/sec. The fan stage has 18 blades, 45 fan exit guide vanes, and 63 core inlet vanes. This fan has a design bypass ratio of 13.3 and its subsonic design tip speed avoids the generation of multiple pure tones. The speed conditions considered, the details of which are provided in Table 1, are representative of the three certification points (approach, cutback, and takeoff), as well as two intermediate fan blade tip speeds.

A. Test Facility and Acoustic Measurements

The 9'x15' wind tunnel, a schematic of which is shown in Figure 3, is an open-loop, continuous-flow, anechoic wind tunnel facility. Acoustic measurements are acquired using a traversing microphone along the sideline placed 89.3 inches (approximately four fan diameters) from the fan axis. Data were taken at 48 positions in 2.5-degree intervals starting at 25° from the fan axis with 0° being the forward position upstream of the fan. Additionally, to obtain more angular coverage in the aft quadrant, three fixed microphone probes are placed in the rear of the test section. Together, the traversing probe and the fixed microphones result in 51 measurement locations that cover sideline emission angles (based on 0.1 Mach number) ranging from 25° to 158° relative to the mid-chord of the fan. All measured and predicted results in the study are referenced to these emission angles, herein also referred to as sideline angles.

In addition to sideline acoustic measurements, a rotating rake¹⁰ measurement system was used to provide a map of the acoustic duct modes present in the fan duct. The system consists of a continuously rotating radial microphone rake that is inserted into the fan duct in such a manner that the pressure profile may be separated into circumferential modes. The radial modes are obtained through a least-squares fit to these circumferential modes using the hard-wall cylindrical Bessel functions as the basis functions.

III. Prediction Code Descriptions

Although more detailed discussions of the codes have been presented elsewhere, a description of the current empirical method included in ANOPP and the new coupled computational approach are provided. After introducing the ANOPP methodology, the individual components of the computational approach and the coupling procedure are described.

A. Aircraft NOise Prediction Program (ANOPP)

NASA introduced the Aircraft NOise Prediction Program⁷ (ANOPP) approximately 30 years ago to provide a capability for predicting the noise from aircraft in flight. ANOPP consists of a set of functional modules that compute atmospheric properties, aircraft flight path, source-to-observer geometry, source noise of the aircraft components (propulsion systems and airframe), propagation of the source noise to ground observers, and community noise metrics. NASA initiated the development of ANOPP to provide the U.S. Government with the ability to independently (1) assess aircraft system noise, (2) assess aircraft component noise, and (3) evaluate aircraft noise technologies and flight procedures. To meet these goals, the prediction methodologies that have been implemented within ANOPP are predominantly empirical or semi-empirical in nature. Many of the prediction methods work well for conventional aircraft designs, but lack capability and fidelity required for non-conventional configurations.

There are a number of modules in ANOPP to model the various aircraft engine and airframe noise sources. The particular source noise module used in this study is the Heidmann Fan Noise (HDNFAN) module found in ANOPP Level 27, version 1. This empirical fan noise module actually contains 3 options for fan noise prediction. The first option is the original Heidmann method which is based on a method developed by the Boeing company and later improved by full-scale data acquired under the direction of M. F. Heidmann¹¹ in 1975. This original method is the foundation for the other 2 options, which are modifications to provide prediction capabilities for fans outside the original database. The second option was developed by Honeywell¹² to improve predictions for small turbofan engines in 2,000 to 6,000 pound full-scale thrust range. The third option was developed by GE Aircraft Engines¹³ to improve predictions for large fans found on engines with full-scale net thrust on the order of 60,000 pounds. To compare with the measured ADP results the GE modification to the original Heidmann method is employed. This method is based on data that is most representative of the ADP design.

HDNFAN predicts five fan noise components; inlet and aft radiated broadband noise, inlet and aft radiated rotor-stator interaction tones, and for supersonic tip speeds, combination tone noise. The effect of inlet distortion and inlet guide vanes are also modeled in this method. The general form of each component noise spectra is given as

$$SPL(f, \theta) \sim 10 \log(p^2(f, \theta))$$

where $p^2(f, \theta)$ is the far-field mean-square acoustic pressure, f is the one-third octave band center frequency, and θ is the sideline angle. The mean-square acoustic pressure for each component is then assumed to have the form

$$p^2(f, \theta) \sim \frac{\tilde{A}^2 \Pi}{4\pi \tilde{r}^2} D(\theta) S(f)$$

where \tilde{A} is the normalized annular flow area at the fan face, \tilde{r} is the normalized source to observer distance, Π is the overall acoustic spectrum level, D is the directivity function, and S is the spectrum shape. The procedure predicts a spectrum shape, spectrum level, and free-field directivity for each of the noise components. The total noise spectrum is then obtained by summing the component spectra on an energy basis. This is done for each sideline angle considered. For this study, only the aft radiated rotor-stator interaction tone component is considered. The spectrum shape, S , is predefined and positioned within the frequency domain based on the blade passage tone frequency of the fan. The spectrum level is determined based on the temperature change across the fan, the mass flow rate, the relative fan tip Mach number, and the rotor-stator spacing. It should be noted that for this method the acoustic directivity function depends only on the sideline angle, θ . The change in fan RPM which could potentially result in a shift in peak directivity is not captured. The peak for the rotor-stator interaction tones will always occur between 120 and 130 degrees independent of the fan operating condition.

B. LINFLUX

In the first step of the coupled computational approach to fan noise source predictions, the LINFLUX^{6, 14} code is used to compute the rotor-stator interaction tones generated as a result of the mean perturbations in the fan rotor wake impinging on the stator. This code provides a frequency-domain, three-dimensional, linearized inviscid description of the unsteady flow. The underlying mean flow (also three-dimensional and inviscid) is representative of the flow through a realistic stator.

Although the required nonlinear mean flow can be computed using any suitable inviscid code, a serial version of the TURBO¹⁴ steady aerodynamic code was used. Subject to this mean flow and specified wake perturbation input, LINFLUX calculates perturbation density, momenta and internal energy everywhere in the domain. In addition to the field solution, the tone sound pressure level and acoustic power level upstream and downstream of the stator are also available. In this study, the objective was to resolve the second^a harmonic of the blade passing frequency (i.e., 2xBPF) tone and predictions for the ADP from a previous assessment of fan noise prediction capabilities were available. An indication of the accuracy of these predictions was obtained by comparison with the aforementioned rotating rake data. Since the computational outflow boundary was well upstream of the rotating rake measurement stations, the data-theory comparisons were made on an acoustic power level basis, which was considered to be conserved, at least for the non-swirling flow downstream of the stator. Comparisons of the downstream-radiated noise (*i.e.* the exhaust noise) for the 2xBPF tone as a function of the tip speed are shown in Figure 4. The predictions agreed with the measurements to within the experimental uncertainty band at lower fan tip speeds, but deviated from the measurements at higher fan tip speeds. The uncertainty margin in the measured tone power level was ± 3.4 dB, which is indicated by the errors

^aThe first blade passage frequency is cut-off given the blade/vane ratio

bars on the experimental data. Note that this uncertainty includes modeling error resulting from the use of hardwall, plug flow duct modes in the rotating rake analysis when shear flow basis functions would be more appropriate. This error was also incurred when the LINFLUX source information was transferred to the duct propagation code.

C. CDUCT-LaRC

To predict sideline acoustic levels and compare with measured data, the predicted fan noise source information from LINFLUX is passed to the CDUCT-LaRC duct propagation and radiation code. This code calculates the propagation of a given acoustic source ahead of the fan face or aft of the exhaust guide vanes in the inlet or exhaust ducts, respectively. Subsequent to the propagation calculations, the code has the capability of computing the noise radiation field outside the duct. CDUCT-LaRC development has been directed toward the efficient modeling of many of the issues that make propagation and radiation analysis in three-dimensional acoustically lined ducts complex. These include:

1. The duct may have a non-uniform circular or annular section. As a result, the flow in the duct may be nonuniform.
2. There may be a pylon and a bifurcation in the exhaust duct resulting in one or two C-shaped regions. This will completely change the character of acoustic wave propagation from that of an annular duct.
3. The acoustic lining on the duct wall may be nonuniform (i.e. circumferentially and radially segmented).

The CDUCT-LaRC code is composed of five distinct modules: 1) input and output specification, 2) Computational Fluid Dynamics (CFD) and acoustic grid generation, 3) background flow calculation, 4) duct acoustic propagation, and 5) duct acoustic radiation. These modules are coupled within a framework to model duct propagation and radiation. All of the modules that currently make up CDUCT-LaRC framework have been discussed previously¹⁵ and are utilized in this study. However, this discussion will focus on the propagation and radiation modules, as they are most pertinent to this investigation.

The duct propagation module is based on the CDUCT code developed by Dougherty^{16,17} and extended by Lan.¹⁸ It utilizes a parabolic approximation to the convected Helmholtz equation and offers a computationally efficient model that accounts for the complexities listed above. The CDUCT-LaRC code has been extended to allow a user to automatically perform multi-block propagation calculations. The grid connectivity is determined and data is transferred from upstream to downstream blocks without user intervention. Results of the propagation module include the acoustic potential or pressure within the duct. These results may then be utilized by the radiation module for acoustic radiation calculations.

The duct radiation module is based on the Ffowcs Williams-Hawkings (FW-H) equation with a penetrable data surface which has been shown to generally provide better results than the Kirchhoff formula for moving surfaces.¹⁹ Based on the background flow conditions and propagation solution on a given source surface, this module calculates the radiated acoustic pressure at various observer locations. The source surface may be taken to be the nacelle inlet or exhaust plane for inlet or aft-fan cases, respectively. Additionally, the effect of the shear layer on the aft radiated noise can also be accounted for within the CDUCT-LaRC framework.^{20,21} In this approach, the CDUCT-LaRC bypass duct propagation calculation is extended to a 'pseudo-duct' beyond the exhaust plane. The outer surface of the 'pseudo-duct' is defined by the shear layer surface upon which a boundary condition similar to an acoustic liner boundary condition is applied. The development of the boundary condition is based on the satisfaction of two conditions:

1. The particle displacement must be continuous across the shear layer.
2. The acoustic pressure must be continuous across the shear layer.

This²⁰ results in an impedance boundary condition on the external surface of the form

$$z_1 = \frac{u_{n2}}{u_{n1}} z_2 \quad (1)$$

where u_n is the acoustic velocity normal to the shear layer, z is the normalized acoustic impedance, and the subscripts 1 and 2 designate regions inside and outside the shear layer, respectively.

IV. Implementation

Before proceeding to a discussion of the results, a few aspects of the coupled LINFLUX/CDUCT-LaRC implementation should be addressed. The first was alluded to previously and involves the specification of mean flow Mach number and source acoustic potential for propagation calculations. Figure 5 illustrates the computational grid topology used in the coupled predictions. The LINFLUX computational domain is shown upstream as a red wireframe grid and is seen to encompass the axial extent of the exit guide vanes^b. The block used for interior duct propagation is shown in green wireframe and the 'pseudo-duct' is shown in blue wireframe at the furthest downstream extent. It can be seen that the source plane for the propagation calculations is located at the outflow boundary of the LINFLUX computational domain. Although non-uniform flows may be considered within CDUCT-LaRC, the mean flow for the current study was assumed to obey a one-dimensional Mach-Area relation. The initial Mach number at the CDUCT-LaRC source plane was obtained by averaging the mean flow over the LINFLUX outflow boundary.

The acoustic potential at the source plane was similarly specified using LINFLUX data. While CDUCT-LaRC can accept arbitrary source specification (*i.e.* it is not a modal code), it is often convenient to specify the acoustic source distribution in terms of duct modes. For situations in which the source pressure is available, this greatly simplifies the conversion to the required acoustic potential. In light of this, the LINFLUX perturbation pressure solution at the outflow boundary was decomposed into hardwall, shear flow duct modes. Resultant modal source information for each of the speeds considered is provided in Table 2. The source acoustic potential distribution was then reconstructed using this modal amplitude and phase information. Hardwall cylindrical Bessel functions were used in this reconstruction, which is consistent with the assumed mean flow profile. Differences between the shear flow and plug flow modes have previously been investigated^{6,14} and neglecting them in this initial investigation was considered acceptable. However, the uncertainty in the source specification must be kept in mind when ultimately comparing predicted and measured results.

A final aspect of the prediction process that warrants further explanation is the implementation of the shear layer model. Following results from previous investigations,^{20,21} the impedance obtained from Equation 1 for the lowest order radial mode at the given circumferential mode, m , was used for all radial modes at that mode number, m . Therefore, in all speed cases considered, the shear layer impedance value for the $m = -9, n = 0$ mode was used for all subsequent radial modes. This meant that only a single impedance value was required and allowed all radial modes to be considered in a single calculation. To qualitatively illustrate the 'pseudo-duct' calculation, an example for the 5425 speed case is shown in Figure 6. Here, contours of the real part of acoustic potential are shown in the interior block and 'pseudo-duct'. The exposed (*i.e.* outer radial and axial) 'pseudo-duct' surfaces are then used as source surfaces for the subsequent FW-H acoustic radiation calculations. In these and subsequent cases, the propagation calculations were performed on an internal computational domain having (25, 176, 65) points and a 'pseudo-duct' domain having (25, 176, 89) points in the radial, circumferential, and axial directions, respectively. This grid resolution was well above that required for the given conditions. However, it was maintained due to the efficiency of the CDUCT-LaRC predictions, as a complete three-dimensional propagation and acoustic radiation prediction took approximately one minute on a single workstation 2.66 GHz CPU.

V. Results and Discussion

Acoustic results are presented at a number of observer locations in addition to the specific sideline locations in the 9'x15' test. For the purpose of assessing the effects of the shear layer and identifying near-field/far-field regions, LINFLUX/CDUCT-LaRC predictions were made on multiple observer arcs centered on the mid-chord of the fan with 180° being the aft downstream position. The radius of each subsequent arc was doubled to more easily identify the acoustic far-field. These calculations also provided the opportunity to investigate the change in directivity due to the inclusion of the shear layer modeling. The next set of results entail comparison of the LINFLUX/CDUCT-LaRC and ANOPP predictions on far-field arcs for aft rotor-stator interaction noise only. These are followed by a final set of results involving the comparison of the LINFLUX/CDUCT-LaRC predictions with the measured sideline data.

A. LINFLUX/CDUCT-LaRC Far-Field Predictions

To identify the acoustic far-field, initial LINFLUX/CDUCT-LaRC predictions were performed on a series of observer arcs centered on the mid-chord of the fan. The radius of the initial arc, R_0 , was specified to be approximately 4 fan diameters (*i.e.* $R_0 \simeq 4D$). Subsequent observer arcs were created by successively doubling the arc radius until a value

^bHere, only one of the 18 fan blades and one of the 45 exit guide vanes are shown to simplify the figure

of $R_5 = 32R_0$ was reached. Two 'pseudo-ducts' having axial extents of approximately 5 and 10 times the annular duct radius ($r_{max} - r_{min}$) were also utilized. The predicted results at aft sideline emission angles are shown in figure 7 (as symbols) for the 5,425 corrected RPM case using the shorter 'pseudo-duct'. Only the aft sideline angles (*i.e.* $90^\circ - 160^\circ$) are included because the specified source is intended to model only the 2xBPF aft rotor-stator tone. The symbols are connected by lines for illustrative purposes only. Near-field effects are present in the first few observer arcs (*i.e.* $\leq R_2 \simeq 16D$), as the character of the directivity pattern continues to change until at least R_3 . A spherical spreading behavior (*i.e.* 6 dB reduction as the radial distance doubles) is observed for arcs of radius R_3 to R_5 . A shift in the peak directivity is also noticeable as the maximum level moves forward from 140° to approximately $120^\circ - 125^\circ$. The 9'x15' measured data was obtained at locations in the range of the R_1 and R_2 arcs and therefore will most likely contain near-field effects.

The presence of the shear layer will affect the far-field directivity pattern. To further illustrate this effect, a comparison of predicted results on R_3 with and without the shear layer is provided in figure 8. It is seen that the shear layer has a refractive effect on the radiated acoustic waves and the predicted peak directivity angle moves forward. Due to the nature of the prediction without the shear layer, sideline angles less than 105° are not included in this figure. Without the inclusion of a 'pseudo-duct', the propagation solution in the duct exhaust plane (*i.e.* the outflow boundary of the CDUCT-LaRC internal propagation block) is taken as the source surface for the FW-H radiation prediction. This leads to predictions that are symmetric about the duct exhaust and not applicable for sideline locations forward of that axial location. When the shear layer is taken into account, the FW-H source surface is comprised of the exposed 'pseudo-duct' surfaces and this situation is avoided. Similar results were obtained for both 'pseudo-duct' lengths and the shorter length was therefore used for subsequent predictions.

B. LINFLUX/CDUCT-LaRC and ANOPP Comparisons

Identification of the acoustic far-field in the LINFLUX/CDUCT-LaRC predictions allows for meaningful comparison with the ANOPP predictions in which far-field assumptions are inherent. Therefore, ANOPP predictions, which included only the aft radiated rotor-stator interaction (Aft RSI) tone component, were made for the ADP at the five speeds previously specified. The predictions for this component followed the same approach and input parameters as those outlined in previous assessment work.⁶ Subsequent comparisons were also made on a one-foot lossless basis for consistency with this previous study. While the LINFLUX/CDUCT-LaRC predictions were carried out for the single 2xBPF frequency, the ANOPP predictions are obtained in one-third octave bands. All of the energy in the one-third octave band containing the 2xBPF frequency was assumed to be associated with the 2xBPF tone.

The results for all five fan speeds are presented in figures 9-11. In these cases, the LINFLUX/CDUCT-LaRC predictions were made on the R_5 arc at one-half degree intervals and are therefore shown as a continuous line and the specific measurement locations identified with circles. These higher resolution predictions were made to more clearly illustrate the details of the directivity pattern. ANOPP predictions were performed only at the measurement locations and are identified with squares.

One feature consistent over the various fan speeds is the lobed character of the LINFLUX/CDUCT-LaRC predictions. This is to be expected due to the nature of the source description. The ANOPP predictions, which are made over one-third octave bands, do not include this source detail in the empirical directivity function. Location and width of the peak directivity are additional features of interest. At the low speeds, the LINFLUX/CDUCT-LaRC and ANOPP predictions are in general agreement. Conversely, at the higher fan speeds, the LINFLUX/CDUCT-LaRC predictions show broader peaks that tend to shift toward aft angles. This characteristic is also absent from the ANOPP predictions due to the fact that the acoustic directivity function does not depend on fan speed.

C. Sideline Data Comparisons

Investigation of the previous far-field predictions indicate that direct comparison of these results with the measured sideline data is not appropriate. For further verification, LINFLUX/CDUCT-LaRC predictions were made at the measurement locations and then projected back to a one-foot arc on a lossless basis. These results were then compared with those obtained on the R_5 far-field arc, as shown in figure 12 for the 5,425 RPM case. Here, the one-half degree increment far-field predictions are again shown as a continuous line and the sideline predictions, which were made at the microphone locations, are identified with circles. The location of peak directivity clearly has shifted forward in the far-field predictions and deviations between the two predictions of up to 10 dB are visible. This indicates that the sideline predictions most likely contain some near-field effects and this behavior was evident over all speed ranges considered. In light of this, for comparison with the measured data, LINFLUX/CDUCT-LaRC predictions at all fan

speeds were made at the measurement locations and projected to a one-foot arc on a lossless basis. The ANOPP predictions are inherently far-field in character and therefore not included in the comparisons with the sideline data.

As with the previous LINFLUX/CDUCT-LaRC and ANOPP comparisons, frequency content and source information must be addressed in comparing with the measured data. Again, the LINFLUX/CDUCT-LaRC predictions were performed at a single frequency (2xBPF) using the rotor-stator interaction tone source information from LINFLUX. The measured data contains contributions from all source components and was obtained in 5.9 Hz bands. In light of this, measured spectra at sideline angles consistent with rotor-stator interaction were investigated. Acoustic levels in the frequency band containing the 2xBPF frequency, and the two adjacent bands, were found to be on the order of 10 dB higher than those in neighboring bands. Therefore, energy in these three frequency bands was taken to belong to the interaction tone. In spite of this attempt to isolate the contribution of the interaction tone, it is important to note that the measured data likely contains contributions from a number of other noise sources.

Bearing in mind the aforementioned points, comparisons between the LINFLUX/CDUCT-LaRC predictions and measured data are presented in figures 13 - 15. An estimated ± 1 dB uncertainty level in the measured data is indicated by error bars and adjacent values are connected by solid lines to more clearly delineate trends in measured and predicted data. The full range of aft sideline angles are presented in 13a to illustrate a baseline data set. However, recalling that only the main interaction ($m = -9$) modes were included in the prediction source (*i.e.* additional modes that may be important are not included), it is the predicted peak levels that are of interest in this initial study. In fact, without including these additional modes, it is problematic to make quantitative comparison between the predicted and measured data at locations away from the peak levels. Previous ADP experimental studies^{8,22,23} showed typical peak acoustic levels to occur in the vicinity of the 136° measurement location. Therefore, subsequent comparison with measured data focused on sideline angles greater than 120°, as seen in figure 13b. For this low speed, good agreement is obtained in both the peak radiation level (within the experimental uncertainty) and location (within approximately 5 degrees). Similar trends are found, with greater deviation in peak level, for the intermediate (6,700 RPM) and cutback (7,525 RPM) fan speeds

Progressing to the high speed cases of figure 15, it is seen that the LINFLUX/CDUCT-LaRC predictions exceed the measured data at large angles for the higher speed. This trend is consistent with the comparison of predicted LINFLUX and measured in-duct acoustic power levels as seen in figure 4. At the higher fan speeds, the LINFLUX predicted in-duct power levels are on the order of 7 dB above the measured values, which in turn contributes to the over-prediction of the sideline acoustic levels. The lobed character of the directivity pattern discussed previously may also lead to some of the discrepancy. However, predictions for the 8,345 RPM case, which showed similar behavior in the far-field, do not appear to be consistent with other results. The source information in table 2 may provide some insight, as an additional radial mode is cut-on at the next (slightly) higher fan speed. However, this is speculative and there is currently no apparent cause for these anomalies at this speed. In general, considering the various assumptions, fair comparison of the peak directivity location is obtained (less than 8 degrees) for fan speeds up to the cutback condition.

VI. Concluding Remarks

In this study, a new coupled computational approach for fan noise prediction was developed and presented. The issues involved in this initial coupling of the LINFLUX and CDUCT-LaRC codes for the prediction the 2xBPF rotor-stator interaction tone of the ADP were discussed. Direct comparison with measured sideline data was problematic at off-peak directivity locations due to the presence of additional sources in the measured data. Overall, fair agreement between the predicted and measured peak directivity levels and locations for fan speeds up to the cutback condition were obtained consistent with the assumed rotor-stator interaction tone source. The coupled LINFLUX/CDUCT-LaRC predictions showed variability with respect to sideline angle and fan speed that was similar to the measured data. These characteristics were not present in the empirical ANOPP predictions. The LINFLUX/CDUCT-LaRC approach also afforded the ability to perform predictions at the microphone locations to account for the possibility of near-field effects in the measured data at the frequencies of interest. This capability was not available in the inherent far-field, one-third octave band ANOPP predictions. These initial comparisons demonstrate that a numerical approach, such as the coupling of LINFLUX and CDUCT-LaRC, can provide an efficient method for the investigation of specific engine noise source mechanisms. Future work will focus on validation and inclusion of additional extraneous modes in the tonal source description and inclusion of other fan sources (*i.e.* broadband rotor-stator interaction).

References

- ¹Nark, D. M., Burley, C. L., Tinetti, A., and Rawls Jr., J. W., "Initial Integration of Noise Prediction Tools for Acoustic Scattering Effects," AIAA Paper 2008-2996, 2008.
- ²Free Field Technologies, Louvain-la-Neuve, Belgium, *MSC.ACTRAN 2005 User's Manual*, 2005.
- ³Eversman, W., "Mapped Infinite Wave Envelope Elements for Acoustic Radiation in a Uniformly Moving Medium," *Journal of Sound and Vibration*, Vol. 224, 1999, pp. 665–687.
- ⁴Lan, J. H. and Breard, C., "Development and Validation of a 3D Linearized Euler Solver," AIAA Paper 2006-2585, 2006.
- ⁵Watson, W. R., Nark, D. M., and Jones, M. G., "Assessment of 3-D Codes for Predicting Liner Attenuation in Flow Ducts," AIAA Paper 2008-2828, 2008.
- ⁶Envia, E., Tweed, D. L., Woodward, R. P., Elliott, D. M., Fite, E. B., Hughes, C. E., Podboy, G. G., and Sutliff, D. L., "An Assessment of Current Fan Noise Prediction Capability," AIAA Paper 2008-2991, 2008.
- ⁷Zorunski, W. E., "Aircraft Noise Prediction Program Theoretical Manual," NASA TM 83199, National Aeronautics and Space Administration, 1982.
- ⁸Dittmar, J. H., Elliott, D. M., and Bock, L. A., "Some Acoustic Results from the Pratt and Whitney Advanced Ducted Propulsor - Fan 1," NASA TM 1999-209049, 1999.
- ⁹Jeracki, R. J., "Comprehensive Report of Fan Performance from Duct Rake Instrumentation on 1.294 Pressure Ratio, 8.06 ft/sec Tip Speed Turbofan Simulator Models," NASA TM 2006-213863, 2006.
- ¹⁰Sutliff, D. L., "Turbofan Duct Mode Measurements Using a Continuously Rotating Microphone Rake," *International Journal of Aeroacoustics*, Vol. 6, No. 2, 2007, pp. 147–170.
- ¹¹Heidmann, M. F., "Interim Prediction Method for Fan and Compressor Source Noise," NASA TM X-71763, 1979.
- ¹²Hough, J. W. and Weir, D. S., "Aircraft Noise Prediction Program (ANOPP) Fan Noise Prediction for Small Engines," NASA CR 198300, 1996.
- ¹³Kontos, K., Janardan, B., and Gliebe, P., "Improved NASA-ANOPP Noise Prediction Computer Code for Advanced Subsonic Propulsion Systems Volume I: ANOPP Evaluation and Fan Noise Model Improvement," NASA CR 195480, 1996.
- ¹⁴Verdon, J. M., "Linearized Unsteady Aerodynamic Analysis of the Acoustic Response to Wake/Blade-Row Interaction," NASA CR 2001-210713, 2001.
- ¹⁵Nark, D. M., Farassat, F., Pope, D. S., and Vatsa, V., "The Development of the Ducted Fan Noise Propagation and Radiation Code CDUCT-LaRC," AIAA Paper 2003-3242, 2003.
- ¹⁶Dougherty, R. P., "A Wave-Splitting Technique for Nacelle Acoustic Propagation," AIAA Paper 97-1652, 1997.
- ¹⁷Dougherty, R. P., "A Parabolic Approximation for Flow Effects on Sound Propagation in Nonuniform, Softwall, Ducts," AIAA Paper 99-1822, 1999.
- ¹⁸Lan, J. H., "Turbofan Duct Propagation Model," NASA CR 2001-211245, 2001.
- ¹⁹Brentner, K. B. and Farassat, F., "Analytical Comparison of the Acoustic Analogy and Kirchhoff Formulation for Moving Surfaces," *AIAA Journal*, Vol. 36, No. 8, 1998, pp. 1379–1386.
- ²⁰Nark, D. M., Farassat, F., Pope, D. S., and Vatsa, V., "A Model for Shear Layer Effects on Engine Noise Radiation," AIAA Paper 2004-2992, 2004.
- ²¹Nark, D. M. and Farassat, F., "CDUCT-LaRC Status - Shear Layer Refraction and Noise Radiation," AIAA Paper 2006-2587, 2006.
- ²²Elliott, D. M. and Dittmar, J. H., "Some Acoustic Results from the NASA/Pratt and Whitney Advanced Ducted Propulsor Model," AIAA Paper 2000-0351, 2000.
- ²³Maria, O. L. S., Soderman, P. T., Horne, W. C., Jones, M. G., and Bock, L. A., "Internal Acoustics Measurements of a Full Scale Advanced Ducted Propulsor Demonstrator," AIAA Paper 1995-3034, 1995.

Condition	Corrected RPM	% Design Speed
Approach	5,425	62.0%
-	6,700	76.6%
Cutback	7,525	86.0%
-	8,345	95.4%
Takeoff	8,750	100.0%

Table 1: ADP Model Fan Tip Speed Conditions

Corrected RPM	m	n	SPL (dB)	Phase (deg)	PWL (dB)
5,425	-9	0	105.5	345.7	102.9
	-9	1	100.2	82.3	95.0
Total			106.6		103.6
6,700	-9	0	112.1	305.4	109.4
	-9	1	103.8	16.6	99.6
	-9	2	102.3	320.2	95.7
Total			113.1		110.0
7,525	-9	0	116.2	283.1	113.3
	-9	1	105.0	2.8	100.8
	-9	2	107.5	256.8	101.9
Total			117.1		113.9
8,345	-9	0	122.7	260.5	119.0
	-9	1	113.7	62.3	109.6
	-9	2	111.2	226.4	106.0
Total			123.4		119.7
8,750	-9	0	125.3	222.4	121.6
	-9	1	121.9	23.2	118.1
	-9	2	118.4	207.9	113.4
	-9	3	95.2	49.7	87.5
Total			127.5		123.7

Table 2: LINFLUX Shear Flow Modal Amplitude and Phase



Figure 1: Advanced Ducted Propulsor (ADP) Model Fan 1 installed in the Low Speed Wind Tunnel.

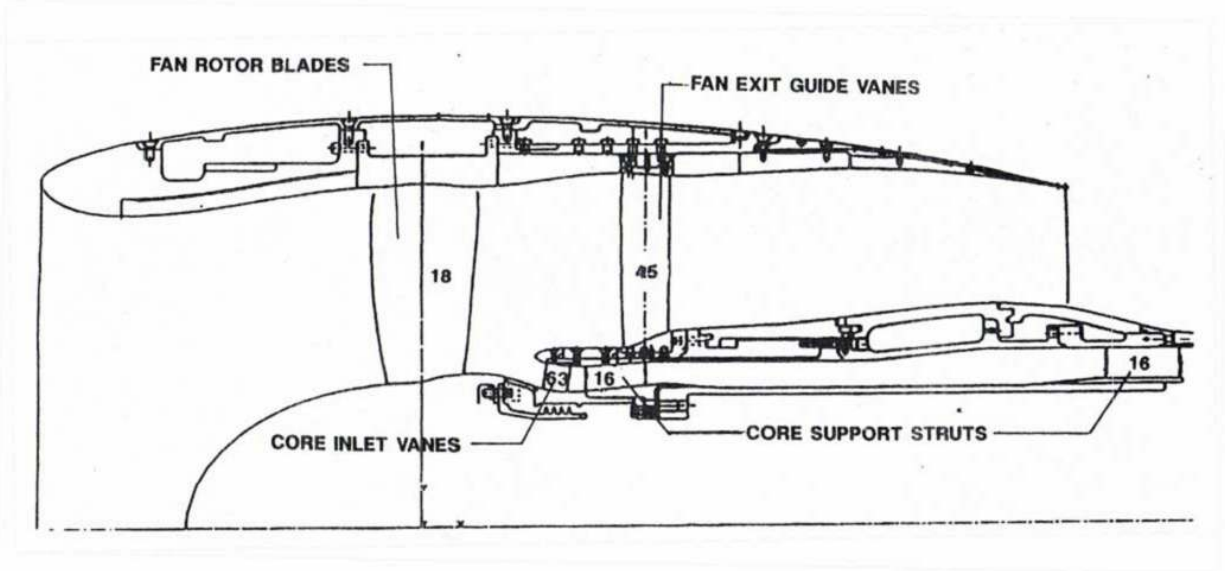


Figure 2: Cross-section of the ADP Fan 1 model fan stage.

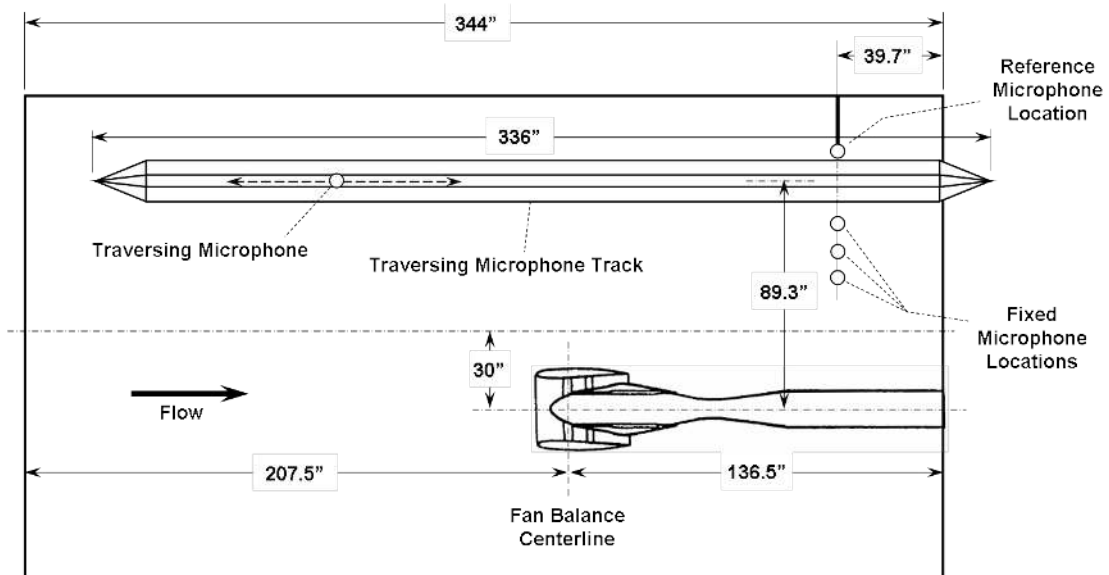


Figure 3: Top view of the 9'x15' test section illustrating model fan installation, as well as traversing microphone and three fixed aft microphones. All dimensions are in inches.

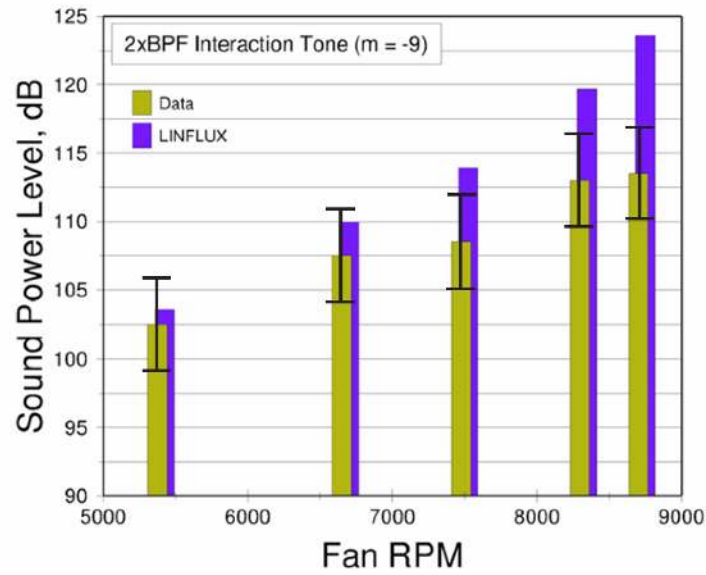


Figure 4: Comparison of predicted (LINFLUX) and measured exhaust rotor-stator interaction tone acoustic power levels for ADP. Results are for the 2xBPF tone for which only the $m = -9$ circumferential mode propagates.

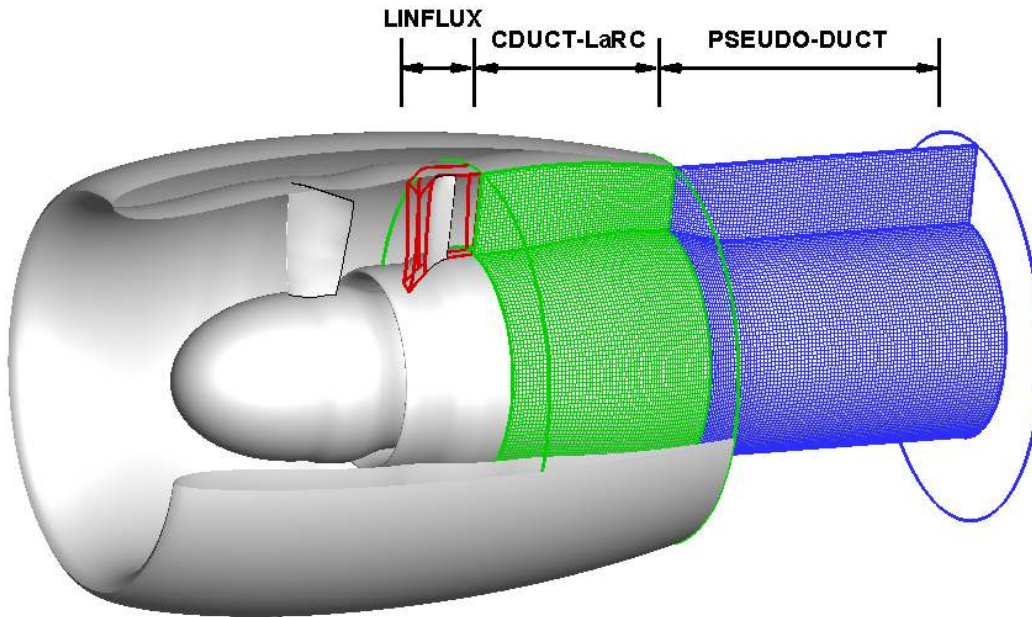


Figure 5: Block topology used for LINFLUX/CDUCT-LaRC predictions. The LINFLUX computational domain is shown in red wireframe. The CDUCT-LaRC internal duct propagation and 'pseudo-duct' blocks are shown in green and blue wireframe, respectively. Note that only one of the fan blades and one of the exit guide vanes are shown to simplify the figure.

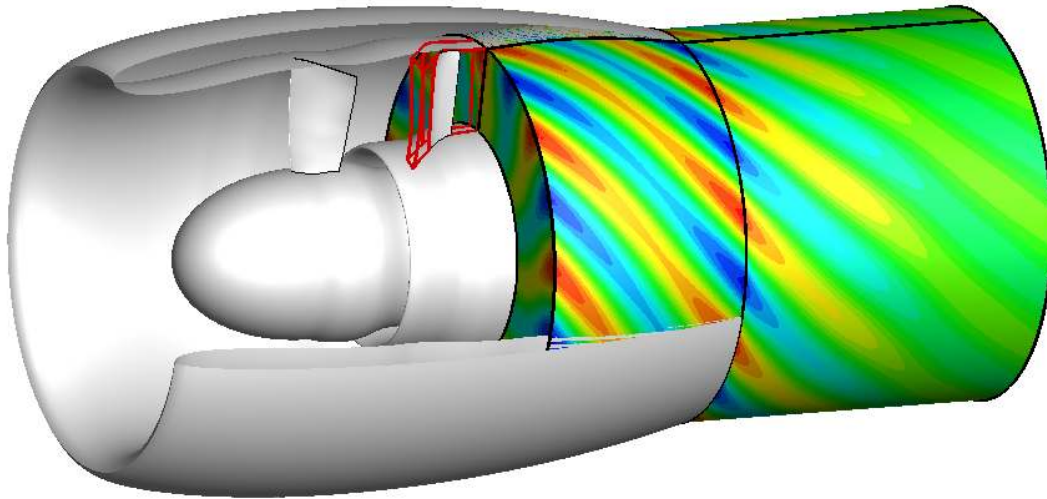


Figure 6: Qualitative acoustic propagation prediction with 'pseudo-duct' showing contours of the real part example of acoustic potential. The exposed surfaces of the 'pseudo-duct' are used as the source surface in subsequent FW-H acoustic radiation prediction.

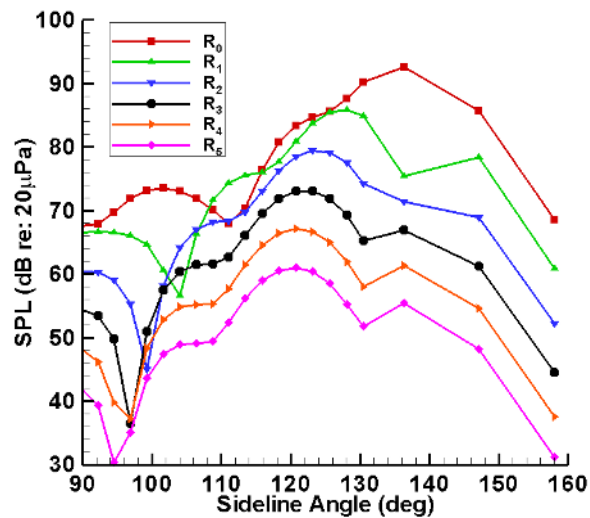


Figure 7: Predicted sound pressure level at 2xBPF for observers on arcs of radius R_0 to R_5 (~ 4 to 128 fan diameters).

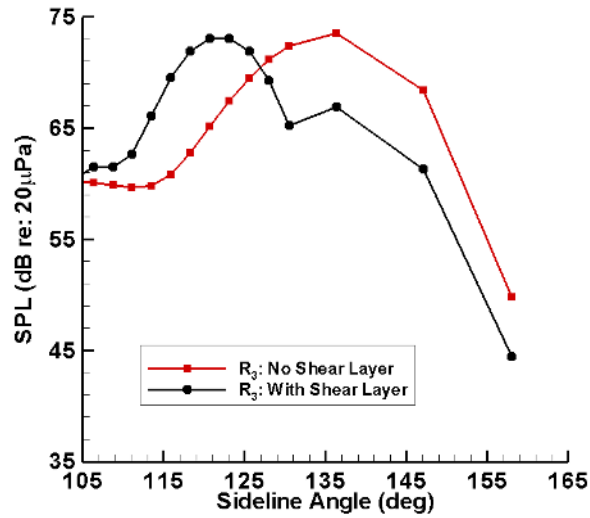


Figure 8: Predicted sound pressure level at 2xBPF for observers on an arc of radius R_3 , with and without shear layer.

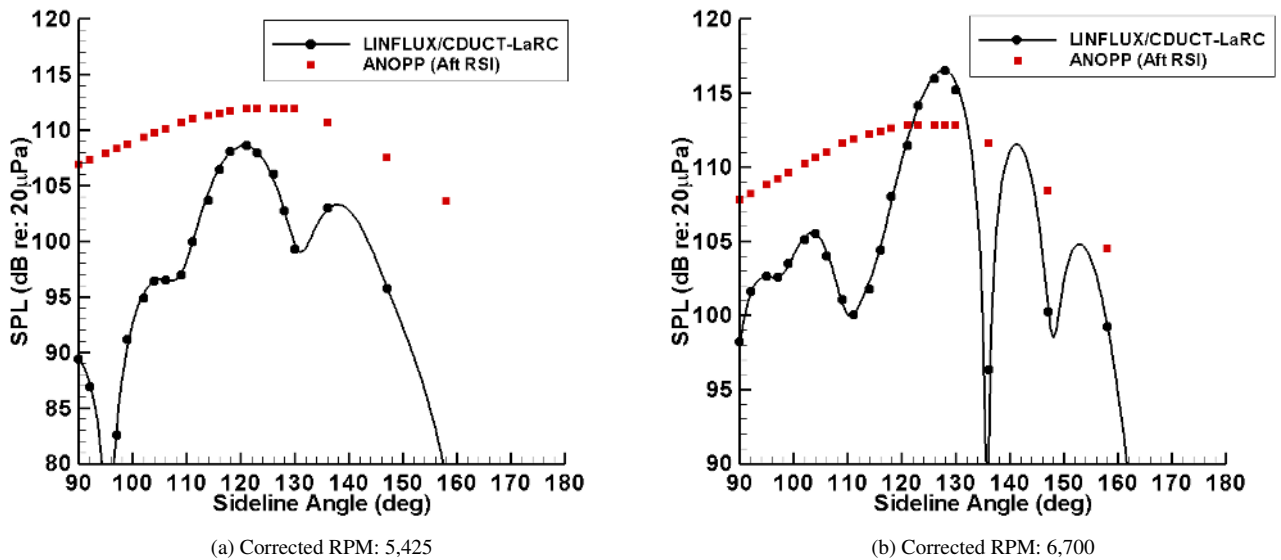
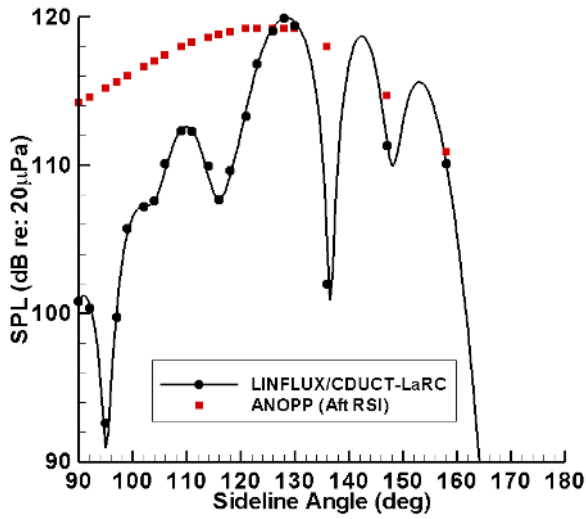
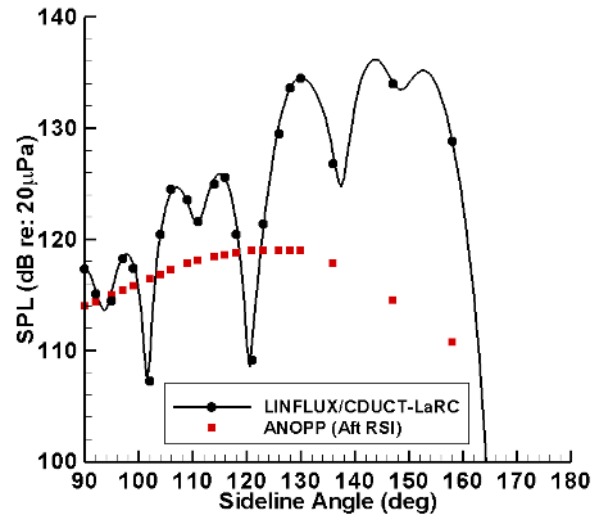


Figure 9: Comparison of far-field LINFLUX/CDUCT-LaRC and ANOPP at 5,425 (Approach) and 6,700 RPM projected to a one-foot arc on a lossless basis. Symbols indicate sideline angles corresponding to microphone locations in 9'x15' sideline measurements.



(a) Corrected RPM: 7,525



(b) Corrected RPM: 8,345

Figure 10: Comparison of far-field LINFLUX/CDUCT-LaRC and ANOPP at 7,525 (Cutback) and 8,345 RPM projected to a one-foot arc on a lossless basis. Symbols indicate sideline angles corresponding to microphone locations in 9'x15' sideline measurements.

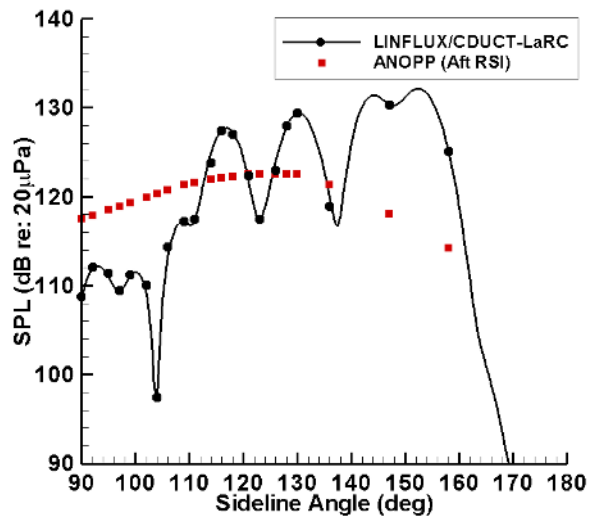


Figure 11: Comparison of far-field LINFLUX/CDUCT-LaRC and ANOPP at 8,750 RPM (Takeoff) projected to a one-foot arc on a lossless basis. Symbols indicate sideline angles corresponding to microphone locations in 9'x15' sideline measurements.

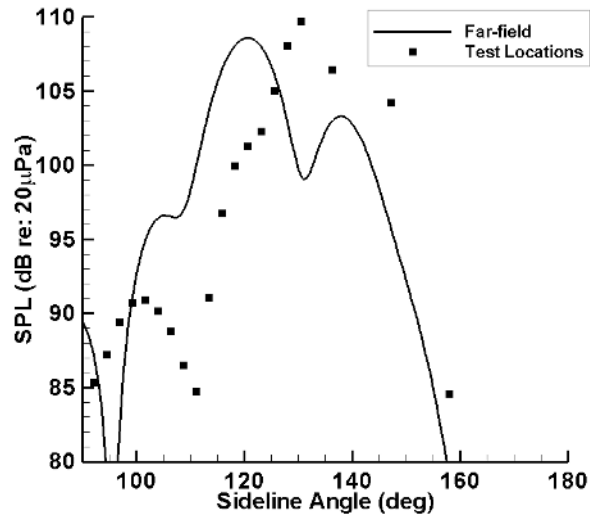
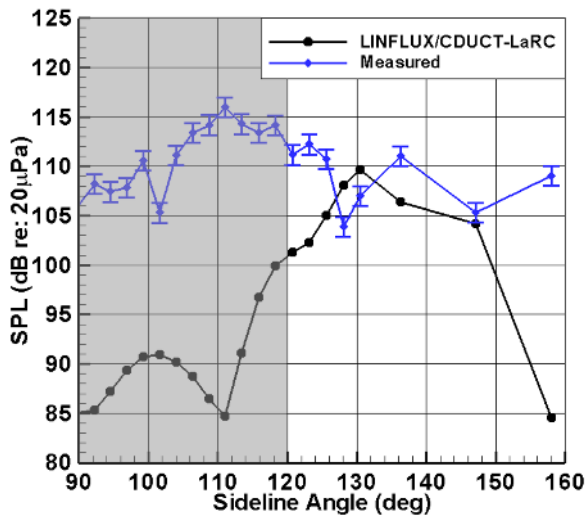
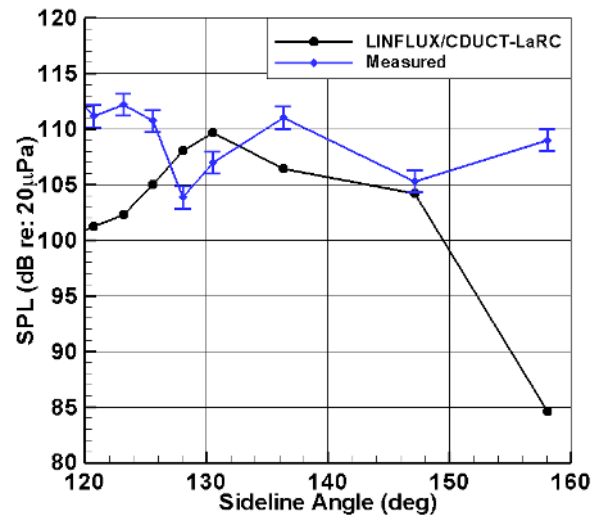


Figure 12: Comparison of far-field (R_5) and sideline (9'x15' measurement locations) LINFLUX/CDUCT-LaRC predictions at 5,425 RPM projected to a one-foot arc on a lossless basis.

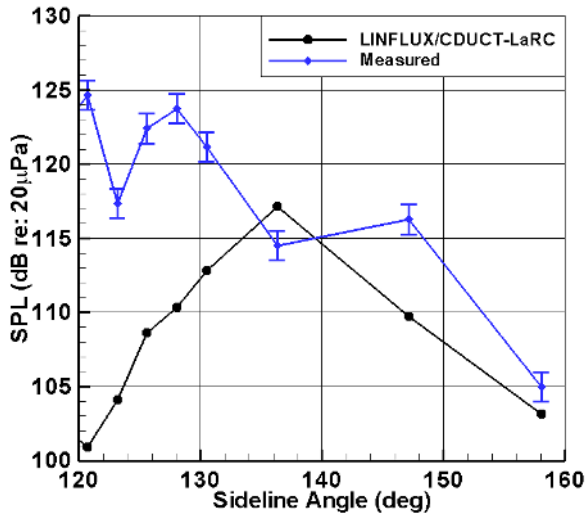


(a) Corrected RPM: 5,425 (Expanded Sideline Angle Range)

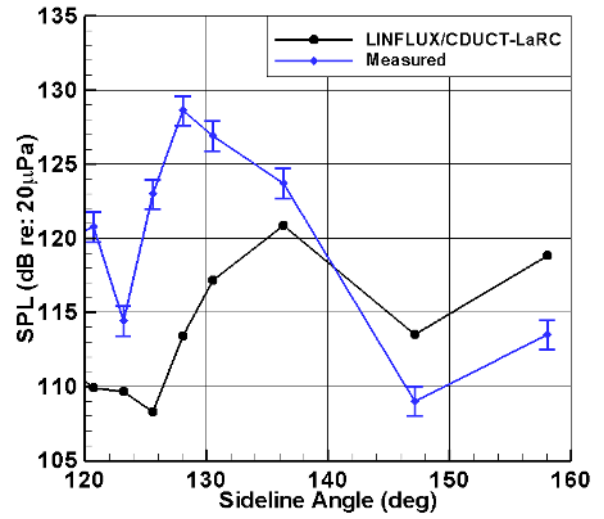


(b) Corrected RPM: 5,425 (Approach)

Figure 13: Comparison of sideline LINFLUX/CDUCT-LaRC predictions with measured data at 5,425 RPM projected to a one-foot arc on a lossless basis.

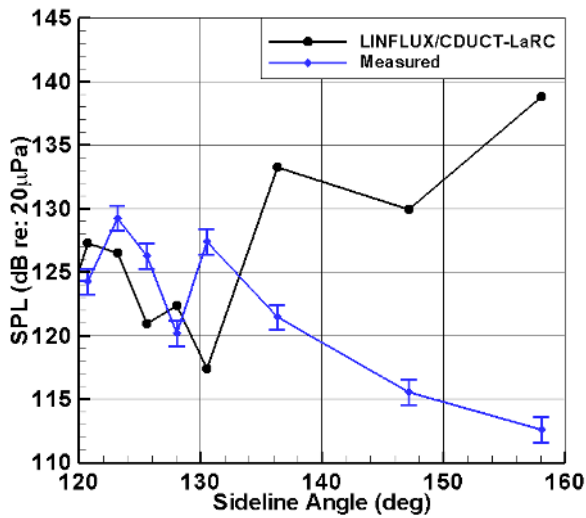


(a) Corrected RPM: 6,700

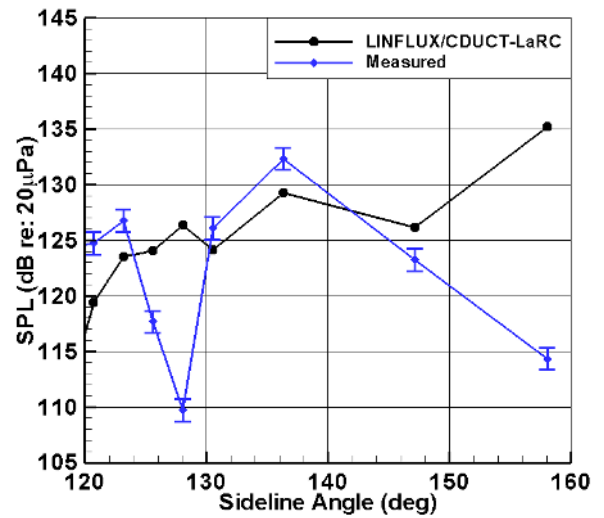


(b) Corrected RPM: 7,525 (Cutback)

Figure 14: Comparison of sideline LINFLUX/CDUCT-LaRC predictions with measured data at 6,700 and 7,525 RPM projected to a one-foot arc on a lossless basis.



(a) Corrected RPM: 8,345



(b) Corrected RPM: 8,750 (Takeoff)

Figure 15: Comparison of sideline LINFLUX/CDUCT-LaRC predictions with measured data at 8,345 and 8,750 RPM projected to a one-foot arc on a lossless basis.